# Dynamic Mathematical Model for Biodegradation of VOCs in a Biofilter: Biomass Accumulation Study

**ARTICLE** *in* ENVIRONMENTAL SCIENCE AND TECHNOLOGY · AUGUST 1998

Impact Factor: 5.33 · DOI: 10.1021/es9711021



**2 AUTHORS**, INCLUDING:

Makram T Suidan
American University of Beirut
**389** PUBLICATIONS **8,470** CITATIONS

SEE PROFILE

*Environ. Sci. Technol.* **1998**, *32,* 3118−3123

# Dynamic Mathematical Model for the Biodegradation of VOCs in a Biofilter: Biomass Accumulation Study

CRISTINA ALONSO AND MAKRAM T. SUIDAN*

*Department of Civil and Environmental Engineering, University of Cincinnati, Cincinnati, Ohio 45221-0071*

BYUNG R. KIM

*Chemistry Department, Ford Research Laboratory, Dearborn, Michigan 48121*

BYUNG J. KIM

*U.S. Army Construction Engineering Research Laboratory, Champaign, Illinois 61820*

Although biofiltration is a firmly established technology for the control of emissions of volatile organic compound (VOCs), more fundamental research is still needed. This work uses a mathematical model describing the dynamic physical and biological processes occurring in a packed trickle-bed air biofilter to analyze the relationship between biofilter performance, biomass accumulation in the reactor, and mathematical description of the packed bed porous media. In this study a biofilter packed with pelletized support media was used to treat toluene achieving removal efficiencies over 99% and 97% for 4.1 and 6.2 kg COD/$m^3$ day toluene loading, respectively. Experimental results showed that as biomass accumulates in the reactor, the available area for the contaminant to diffuse into the biofilm decreases causing a drop in removal efficiency. This effect is specially important for biofilters where there is a high degree of biomass accumulation that significantly affects biofilter performance. In response to these observations, a new approach for the calculation of the biofilm specific surface area of the reactor as a function of biomass growth was developed. Three models of the reactor porous medium were analyzed. The medium was represented as a bed of equivalent spheres in the first model, as an equivalent set of parallel pipes in the second model, and as an equivalent set of flat parallel plates in the third model. The first two models, spheres and pipes, were proven superior in their ability to explain the system performance. The effect of contaminant solubility on biofilter performance was also analyzed.

## Introduction

Due to regulatory demands, there is growing interest to control the emission of VOCs into the environment. Biofiltration has been proven to be a cost-effective technology in the removal of VOCs and other pollutants from waste gas streams. A biofilter consists of a packed bed of organic or synthetic materials on which microbial films are supported. Biodegradable pollutants present in a waste gas pass through a biofilter, diffuse through microbial films, and are consumed. Although extensive experimental and theoretical research has been done in this field, biodegradation is not yet a mature technology. Because of the complexity of the processes occurring in a biofilter, more fundamental knowledge is necessary to extrapolate experimental results to the development of general design criteria. Much research has focused on understanding this process through theoretical models. This study presents a fundamental mathematical model of the VOC degradation process that can be used as a tool for biofilter design and performance prediction.

Many researchers have modeled gas biofilters. The model of Jennings et al. (*1*) was first adapted to the gas-phase biofilter by Ottengraf and Van der Oever (*2*). Recently, air biofilter models have been introduced that account for more detailed representations of biofilm biodegradation mechanisms (*3*−*7*). Zarook et al. (*5*) and Deshusses et al. (*6, 7*) calculated the transient contaminant concentration, but they assumed that the biofilm thickness and the biomass density were constant in time. In this work, the modeling description of dynamic performance of synthetic media trickle-bed biofilters presented in Alonso et al. (*8*) is further expanded and complemented with new features.

This mathematical model was developed in support of experimental results from the operation of a pilot-scale trickle-bed gas biofilter (*8*−*10*) packed with pelletized biological support media. Although previous models assumed that the biofilter reaches steady state, these results showed changes in biofilter performance with time due to the variation in the amount of biomass present in the system. The contaminant removal efficiency increased and then decreased while biomass was accumulating in the reactor. The initial improvement in the performance was easily explained, since an increase in the mass of microorganisms results in increased contaminant removal potential. The subsequent drop in the removal efficiency was a consequence of the reduction in the specific surface area of the biofilm that accompanies biomass accumulation. Biomass was assumed to grow by filling the void fraction between the packing solids, which decreases the available area for the contaminant to diffuse into the biofilm and therefore the removal efficiency. Thus, the assumption of steady state biofilm thickness was not appropriate and a dynamic model was needed. This conclusion applies specially in the case of biofilters with a high biomass growth, as in this work, where the loss of specific surface area significantly affects biofilter performance. The variation of the reactor specific surface area with biofilm thickness was a function of the reactor attachment medium. Porous media models were used to describe the packed bed. Three different models were evaluated. In the first one, the randomly packed bed was modeled as a bed of regularly packed equivalent spheres. The other two models represented the irregular media pores as equivalent parallel pipes and as equivalent parallel plates, respectively. The mathematical model was then used to analyze the effect of the water layer, nutrient recycle, and contaminant solubility on reactor performance.

## Methodology

**Experimental Setup.** The biofilter used in this study was a stainless steel reactor packed with pelletized diatomaceous

* Corresponding author phone: (513)556-3695; fax: (513)556-2599; email: msuidan@boss.cee.uc.edu.



S0013-936X(97)01102-4 CCC: $15.00 
Published on Web 08/26/1998

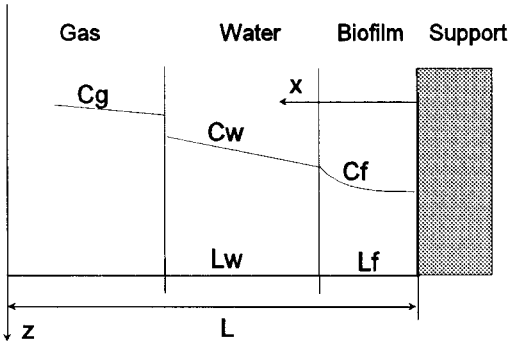


**FIGURE 1. Biofilm model representation.**

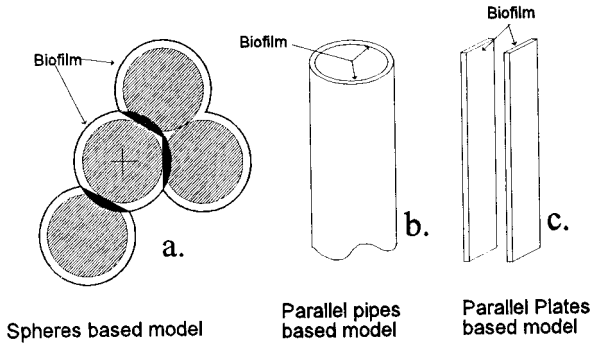


**FIGURE 2. Three physical representations of the packed bed reactor porous media.**

earth biological support media (6 mm R-635 Celite) to a depth of 114 cm. The pelletized medium was selected after initial screening revealed it to be superior to two other candidate media (*9*). The average size of the packing solids was 6 mm in diameter and 4 mm in length. The organic feed to the biofilter consisted of a solution of toluene volatilized in the influent air stream. Before the addition of toluene, the feed air was purified and contained only oxygen and nitrogen. The biofilters were fed 20 L of an aqueous solution of nutrients per day. Nitrate was used as the sole nitrogen source. The temperature of the reactors was 32 °C, and the outlet pressure was very close to atmospheric pressure. The biofilters were operated in a co-current mode. Two different loadings, 4.1 and 6.2 kg COD/$m^3$ day, were used. The initial toluene concentration and Empty Bed Retention Time (EBRT) were 250 and 500 ppmv and 2, 1, 1.33, and 0.67 min. Concentrations of toluene were measured using a gas chromatograph (GC, HP 5890, Series II, Hewlett-Packard, Palo Alto, CA). More detailed description of the experimental apparatus and analytical methods can be found in Sorial et al. (*9*), Smith et al. (*10*), and Alonso et al. (*8*). To remove the excess of biomass that causes the contaminant removal efficiency to drop, the reactor was backwashed regularly with full media fluidization.

**Mathematical Model.** A mathematical model has been developed for a trickle bed biofilter packed with uniform synthetic solids. All processes are assumed to be uniform across the biofilter cross section, and wall and end effects are neglected. The temperature in the biofilter and the physical properties of the gas and VOC are assumed to be constant. Three phases are considered in the system: biofilm, liquid, and gas. The liquid layer is present due to a small and intermittent nutrient solution feed rate. This nutrient solution can be totally or partially recycle. The transient or dynamic model is solved using two geometric dimensions, $x$ perpendicular to the biofilm support and $z$ along the biofilter. One limiting substrate and homogeneous biomass are considered. The variables of interest are the VOC concentration profiles in the biofilm, water, and gas phase, the thickness of the biofilm along the reactor, and the variation of the specific surface area with biomass accumulation. In the formulation of the mass balance equations, the following assumptions are made: the biofilm is a stagnant phase; axial diffusion is negligible; the microbial growth is described by Monod kinetics; VOC is the only growth limiting substrate; the kinetic parameters and bacterial density in the biofilm are constant; and there is no contaminant degradation in the water and gas phases. The biofilm representation is in Figure 1.

Three different representations of the randomly packed bed porous media are analyzed. Figure 2 represents these geometries when biofilm is growing on the media. In the first model, Figure 2a, the random packed bed is modeled as a bed of regularly packed equivalent spheres sized to have the same volume. Due to the random packing, the flow path for the waste gas is considerably tortuous, and the gas is assumed to be well mixed across the biofilter cross section. Therefore, the concentration of contaminant in the bulk gas is considered uniform at any given axial position. The second model, Figure 2b, describes the pores that constitute the porous media as equivalent parallel pipes with the biofilm growing inside the pipes. The concentration of the VOC in the gas phase can be assumed to be uniform or nonuniform in the pipe cross section. In the third model, Figure 2c, the pore is modeled as the opening between two parallel plates with the biofilm covering the inside face of the plates. Spherical, cylindrical, and Cartesian coordinates are used for the spheres, pipes, and parallel plates models, respectively. The equations for Cartesian coordinates corresponding to Figure 1 are formulated here. Equation formulation for the other coordinate systems is immediate.

Equation 1 describes the mass balance equation for the biofilm phase and the boundary condition given by the assumption of no flux of contaminant into the substratum

$$\frac{\partial C_f}{\partial t} = D_f \frac{\partial^2 C_f}{\partial x^2} - \frac{\mu_m X_f}{Y}\left[\frac{C_f}{K_s + C_f}\right]$$

$$@x = 0, \quad \frac{\partial C_f}{\partial x} = 0 \qquad (1)$$

where $C_f$ is the VOC concentration in the biofilm, $D_f$ the contaminant diffusivity in the biofilm, $\mu_m$ the maximum bacterial growth rate, $Y$ the yield coefficient, $K_s$ the Monod saturation constant, and $X_f$ the film bacterial density. $D_f$ is assumed to be a fraction of the diffusivity in water, $D_w$. The mass balance equation for the water phase and boundary conditions in the biofilm−water interface are

$$\frac{\partial C_w}{\partial t} = D_w \frac{\partial^2 C_w}{\partial x^2} - v_w \frac{\partial C_w}{\partial z}$$

$$@x = L_f, \quad C_f = C_w, \quad -D_f \left.\frac{\partial C_f}{\partial x}\right|_{x=L_f} = -D_w \left.\frac{\partial C_w}{\partial x}\right|_{x=L_f} \qquad (2)$$

where $C_w$ is the VOC concentration in the water, $v_w$ the water velocity, and $L_f$ the biofilm thickness. The boundary conditions assume uniform concentration and flux at the biofilm-water interface.

Radially across the bed, the VOC concentration in the gas phase, $C_g$, can be considered uniform or nonuniform. In the case of uniform concentration plug flow is assumed. The mass balance equation and the gas−water interface boundary condition are then expressed as functions of the flux of VOC

into the water layer, $J_w$, and the water−gas interfacial surface area per unit bed volume, $a_f$

$$\frac{\partial C_g}{\partial t} = -u_0\frac{\partial C_g}{\partial z} - J_w a_f$$

$$@x = L_f + L_w, \quad C_g = HC_w, \quad J_w = D_w\frac{\partial C_w}{\partial x} \qquad (3.a)$$

where $u_0$ is the gas approach velocity, i.e., the gas flow rate divided by the biofilter cross-sectional area, and $L_w$ is the thickness of the water layer. The boundary condition is obtained assuming that the VOC concentrations in the water and gas at the interface are in equilibrium as defined by Henry's law. $H$ is the contaminant Henry's constant.

If nonuniform concentration of VOC in the gas phase across the biofilter is assumed, the mass balance equation in the gas phase (eq 3.b) is similar to the one in the water phase (eq 2). The boundary conditions are derived assuming Henry's law, uniform flux of contaminant in the gas−water interface, and no flux of contaminant in the center of the pipe or channel

$$\frac{\partial C_g}{\partial t} = D_g\frac{\partial^2 C_g}{\partial x^2} - v_g\frac{\partial C_g}{\partial z}$$

$$@x = L_f + L_w, \quad C_g = HC_w, \quad -D_g\left.\frac{\partial C_g}{\partial x}\right|_{x=L_f+L_w} = -D_w\left.\frac{\partial C_w}{\partial x}\right|_{x=L_f+L_w}$$

$$@x = L, \quad \frac{\partial C_g}{\partial x} = 0 \qquad (3.b)$$

where $D_g$ is the contaminant diffusivity in the gas phase, $v_g$ the gas velocity in the $z$ direction, and $L$ the radius of the pipe or half the distance between the two plates, depending on the model used.

Assuming uniform VOC gas concentration at the inlet of the biofilter, $C_{g0}$, the boundary conditions in $z$ for eqs 2 and 3 is given by

$$@z = 0 \quad C_g(x,0,t) = C_{g0} \quad C_{w0}H = C_{g0} \qquad (4)$$

The variation of the biofilm thickness with time is due to the net bacterial growth

$$\frac{\partial L_f}{\partial t} = \left(r_d D_w\left.\frac{\partial C_f}{\partial x}\right|_{x=L}\right)\frac{Y}{X_f} - L_f b \qquad (5)$$

where $b$ is the specific shear/decay coefficient. Initial conditions are necessary for all the variables.

**Gas and Water Flow Velocities.** The expressions for the gas-phase axial velocity are calculated assuming flow through a pipe or through a channel with parallel walls and a falling film for the water phase velocity. The gas velocity is

$$v_g = 2(\bar{v}_g - v_i)\left[1 - \left(\frac{L - x}{L - L_f - L_w}\right)^2\right] + v_i, \quad \bar{v}_g = \frac{Q_g}{A\epsilon_f} \quad v_i = \frac{3}{2}\bar{v}_w \qquad (6)$$

where $\bar{v}_g$ is the average gas velocity calculated as the interstitial velocity in porous media, $v_i$ the gas−water interface velocity, $A$ the reactor cross sectional area, $Q_g$ the gas flow to the reactor, and $\epsilon_f$ the packed bed porosity. The water velocity and the average water velocity $\bar{v}_w$ are

$$\bar{v}_w = \bar{v}_i\left[1 - \left(\frac{L_f + L_w - x}{L_w}\right)^2\right], \quad \bar{v}_w = \frac{Q_w}{a_0 A L_w} = \frac{\rho_w g L_w^2}{3\mu_w} \qquad (7)$$

where $Q_w$ is the water flow to the reactor, $\mu_w$ and $\rho_w$ the viscosity and density of water, and $g$ the gravitational constant. $\bar{v}_w$ is calculated in two different ways: as the water flow over the wetted area and by integrating the expression of the water velocity. Combining both expressions, $L_w$ is

$$L_w = \left(\frac{Q_w 3\mu_w}{a_0 H_T \rho_w g}\right)^{1/3} \qquad (8)$$

The system equations can be easily derived for the case when the water layer is neglected.

**Shear/Decay Coefficient Calculation.** Following the formulation of Rittmann (*11*), the combined shear/decay coefficient represents biomass loss and combines biomass decay and physical shearing. The specific decay coefficient, $b_d$, is assumed to be constant, and the specific shear rate, $b_s$, is a function of the biofilm thickness:

$$b = b_s + b_d \qquad (9)$$

The different existing expressions to define the rate of biofilm detachment suggest that this process is not very well understood (*12*). Here, the shear rate is assumed to be proportional to the shear stress on the biofilm surface, $\tau$. If the model includes a water layer, the shear stress is due to the water flow; if there is no water layer, it is due to the gas flow. The expressions for both cases are

$$b_s \alpha \tau \rightarrow b_s = \beta\rho_w g L_w, \ (water) \quad b_s = \beta\left(\frac{\bar{v}_g}{\epsilon_f}\right) = \beta\left(\frac{u_o}{\epsilon_f^2}\right) \ (gas) \qquad (10)$$

The proportionality constant, $\beta$, is chosen by defining a default shear rate coefficient, $b_s0$, corresponding to the default shear stress when the bed is clean and no biofilm is present. Then

$$b = b_{s0} + b_d, \ (water) \quad b = b_{s0}\left(\frac{\epsilon_0}{\epsilon_f}\right)^2 + b_d \ (gas) \qquad (11)$$

**Specific Surface Area and Porosity Calculation.** The three porous media models represent the same packed bed, so the clean (no biofilm) bed porosity and specific surface area is the same for all of them. The clean bed porosity, $\epsilon_0 = 0.34$, is a property of the porous media and is calculated experimentally. To calculate the biofilm surface area per unit volume of clean biofilter, $a_0$, the packing solids are represented by equivalent spheres of a 6 mm diameter, sized to have the same volume as the actual media. A sphericity factor, $\phi = 0.857$, is calculated as the ratio of the surface of the equivalent sphere to the surface of the pellet. Then $a_0$ is

$$a_0 = \frac{3(1 - \epsilon_0)}{\phi R_p} \qquad (12)$$

The calculation of the reactor specific surface area, $a_f$, and porosity, $\epsilon_f$, with biofilm growth depends on the physical representation of the packed bed. In the packing spheres model, the biomass will only grow in the void space left between the solids. The variation of the reactor surface area and porosity with biomass growth depends on the number of spheres in contact with a given one, $n$. For regular packing,

the number of points of contact between a given sphere and the adjacent spheres is called coordination number. This situation is presented in Figure 2a. If $A_L$ and $V_L$ are the biofilm surface area and volume lost with each point of contact, the biofilm specific surface area is given by

$$a_f = \frac{4\pi(R_p + L_f + L_w)^2 - nA_L}{\frac{4}{3}\pi R_p^3}(1 - \epsilon_0) = \frac{a_0}{2}\left(1 + \frac{L_f + L_w}{R_p}\right)\left((2 - n)\frac{L_f + L_w}{R_p} + 2\right) \quad (13)$$

The bed porosity with biofilm can be calculated in the same way:

$$\epsilon_f = 1 - \frac{\frac{4}{3}\pi(R_p + L_f + L_w)^3 - nV_L}{\frac{4}{3}\pi R_p^3}(1 - \epsilon_0) = 1 - (1 - \epsilon_0)\left[\left(1 + \frac{L_f + L_w}{R_p}\right)^3 - \frac{n}{4}\left(\frac{L_f + L_w}{R_p}\right)^2\left(2\frac{L_f + L_w}{R_p} + 3\right)\right] \quad (14)$$

For $n > 4$, the specific surface area and porosity decrease with increasing biofilm thickness, explaining the drop in biofilm performance with excessive biomass accumulation. After reaching certain biofilm thickness, the benefit due to additional biomass is overshadowed by the decrease in specific surface area available for contaminant transport. The value of $n$ can be estimated using (*13*)

$$\epsilon = 1.072 - 0.1193n + 0.004312n^2 \quad (15)$$

In this case, for a clean bed porosity $\epsilon_0 = 0.34$ $n$ is between 9 and 10. 10 was used in the model.

For the equivalent parallel pipes model (Figure 2b), the biofilm grows inside the pipe covering the walls, so the specific surface area and porosity decrease with increasing biofilm thickness:

$$a_f = a_0\left(1 - \frac{L_f + L_w}{L}\right), \quad \epsilon_f = \epsilon_0\left(1 - \frac{L_f + L_w}{L}\right)^2 \quad (16)$$

$L$, the radius of the equivalent pipe, is calculated from the clean bed specific surface area and porosity:

$$L = 2\frac{\epsilon_0}{a_0} \quad (17)$$

For the model based on equivalent parallel plates (Figure 2c), the biofilm grows covering the walls, so $a_f$ does not change with time. $\epsilon_f$, decreases with biofilm growth because the opening between the plates decreases. $L$ is half the distance between the two parallel plates.

$$a_f = a_0, \quad \epsilon_f = \epsilon_o\frac{L - L_f - L_w}{L} \quad L = \frac{\epsilon_0}{a_0} \quad (18)$$

**Numerical Solution.** With this formulation, the problem consists of a three dimension ($x$, $z$, and $t$) system of coupled partial differential equations, which is solved using finite differences equation discretization. A computer program has been written in C to solve this problem. One factor to consider is the characteristic time of the processes. Since the time variation of the biofilm thickness is slower than the variation of the VOC concentrations, the dynamic solution of the system of equations can be simplified using a quasi-steady state solution. Concentration profiles are calculated assuming a fixed biofilm thickness, and biofilm thickness is calculated assuming steady state concentration profiles. In this study, both problems are solved. The time step has to be very small in the solution of the general dynamic problem for stability and convergence of the numerical method. The solution of the quasi-steady state problem is faster because the time step can be larger. Since both solutions are not significantly different, the second method is used without loss in accuracy to save computational time.

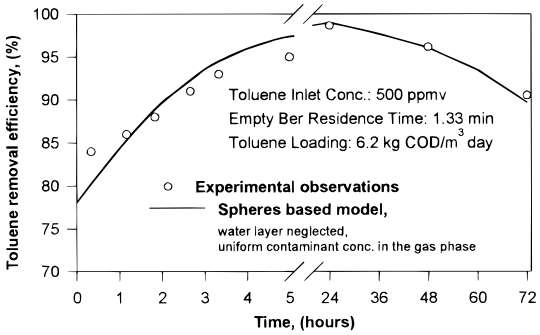


**FIGURE 3. Typical biofilter response with time.**

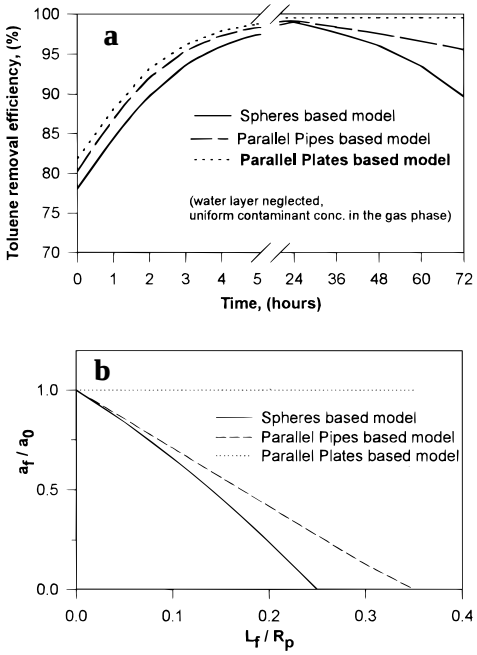


**FIGURE 4. Comparison of the three reactor models. (a) Simulation of biofilter performance after backwashing and (b) variation of the reactor specific surface area with biofilm thickness.**

As the model does not account for inactive biomass, the biofilm substrate concentration is limited by equal growth and decay rates, the minimum concentration needed to maintain the biofilm.

## Results and Discussion

The unknown parameters of the system were previously estimated using experimental data collected in a variety of operational scenarios and nonlinear parameter estimation techniques. A detailed description can be found in Alonso et al. (*8*). The spheres based model was used neglecting the water layer during the parameter estimation. The estimated parameters were yield coefficient ($Y = 0.84$ mg VSS/mg VOC), maximum growth rate ($\mu_m = 3.0$ day$^{-1}$), Monod constant ($K_s = 0.15$ mg VOC/L), default shear rate coefficient ($b_{so} = 0.005$ day$^{-1}$), decay rate coefficient ($b_d = 0.432$ day$^{-1}$), biomass density ($X_f = 17$ g biomass/L), initial biofilm thickness ($L_{f0} = 0.0039$ cm), and biofilm/water diffusivity ratio ($r_d = 0.9$).

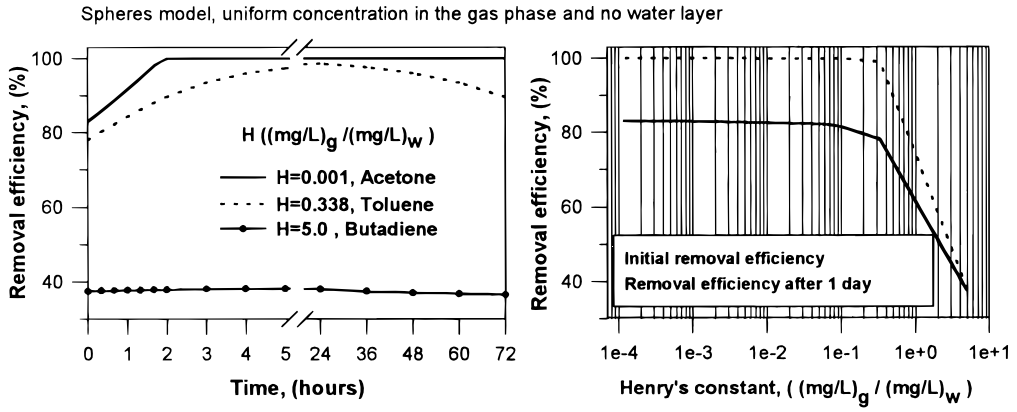


**FIGURE 5. Effect of the variation in the value of the Henry's constant of the contaminant.**

Other input parameters needed in the model were toluene diffusivity in water ($D_w = 10^{-5}$ cm$^2$/s), and toluene Henry's constant ($H = 0.338$ (mg/L)$_{gas}$/(mg/L)$_{water}$).

The characteristic performance of the biofilter during the period between backwashings is presented in Figure 3. Experimental data and model predictions are shown. These results correspond to a biofilter loaded with 6.2 kg COD/m$^3$ day toluene, 500 ppmv initial concentration, and 1.33 min EBRT, backwashed twice a week for 2 h. The initial time corresponds to the moment when the reactor is started after backwashing. The figure shows an initial increase and a subsequent drop in the contaminant removal efficiency while biomass is accumulating in the system. The removal efficiency would typically decrease after the first day of continuous operation. Monod kinetics and mass transfer models alone cannot explain this behavior because they predict an increase in contaminant removal if the biomass quantity increases. The decrease in specific surface area available for contaminant transport into the film with biofilm growth is responsible for this behavior. Figure 3 shows that the mathematical model derived can simulate the dynamic biofilter performance.

With these parameter values, simulations were carried out to compare the three packed-bed reactor models and see which one was best suited to describe the dynamic response of the trickle bed biofilter. The results for the three different models are in Figure 4a. The spheres and pipes based models can predict the decrease in biofilter performance after 1 day, while steady removal efficiency is reached with the parallel plates representation. This difference in reactor response is due to the variation of the reactor specific surface area with biofilm thickness (eqs 13, 16, and 18). Dimensionless surface area is plotted against the dimensionless biofilm thickness in Figure 4b. $a_f$ decreases with biofilm thickness in the spheres and pipes models and is constant in the parallel plates model. The parallel plates based representation is not appropriate to model the packed bed biofilter when biomass accumulation is expected to influence the performance of the system. Figure 4b also shows that the surface area for the pipes based model is higher than for the spheres model, which explains the higher removal efficiency. This difference is due to the irregularity of the packing. For regular packing, both models give similar results. In conclusion, both equivalent spheres or pipes based models can be used to describe the system, and the parallel plates model is not recommended.

Simulations have been performed when the concentration of contaminant in the gas phase is assumed to be uniform and nonuniform in the reactor cross sectional area, for the equivalent pipes and parallel plates models. The results showed that the change in concentration across the gas phase was minimal, so the mass transfer resistance in the gas phase can be neglected in this case.

Another point to consider is the presence of a water phase in the reactor due to the application of nutrient solution. Program simulations showed a lower removal efficiency when the liquid phase was included in the model for a water flow of 20 L/day. The importance of the resistance offered by the water layer to the transport of the contaminant should be analyzed for each particular application.

An important variable in the removal efficiency of a gas biofilter is the value of the compound Henry's constant, because it determines its solubility in water and, therefore, in the biofilm. Figure 5 presents the results of the model simulations when the value of Henry's constant is varied and the rest of the parameters are not changed. Three compounds are shown: butadiene, very insoluble and high value of Henry's constant; toluene, moderately soluble; and acetone, very soluble and low value of Henry's constant. High solubility in water means high removal efficiency, because the compound is more available for bacterial growth. The second plot of Figure 5 shows that for values of $H$ less than approximately 0.01, the reactor removal efficiency does not change with $H$.

The last study is the effect of the recycle of the nutrient flow on biofilter performance. $X$ is the fraction of water flow recycled ($0 \leq X \leq 1$). In this discussion, the biofilter performance is characterized as the contaminant removal efficiency (eff) in percentage. If some nutrient solution is discharged, the water carries out some dissolved contaminant that has not been degraded, so it is questionable whether it should be included or not in the definition of reactor contaminant removal efficiency. One approach is to consider two definitions of efficiency when the water layer is included in the model, one based in the amount of contaminant removed from the gas phase (effA), and the other based in the amount of contaminant biologically degraded (effB). If the water layer is neglected, the removal efficiency is effA

$$\text{effA (\%)} = \frac{M_{gi} - M_{ge}}{M_{gi}} 100, \text{ effB (\%)} = \frac{M_{gi} - (M_{ge} + M_{we})}{M_{gi}} 100 \quad (19)$$

where $M_{gi}$ is the mass of contaminant in the influent gas phase, $M_{ge}$ the mass of contaminant that leaves the biofilter in the effluent gas, and $M_{we}$ the mass of contaminant discharged in the water. Figure 6 shows the simulation of the reactor performance with and without water layer and with no water recycled ($X = 0$). Two compounds are analyzed: toluene, moderately soluble and acetone, very soluble. Because the amount of toluene dissolved in water is very low, the value of the two definitions of reactor efficiency is very similar when the water layer is included, and this efficiency is lower than the efficiency obtained when the

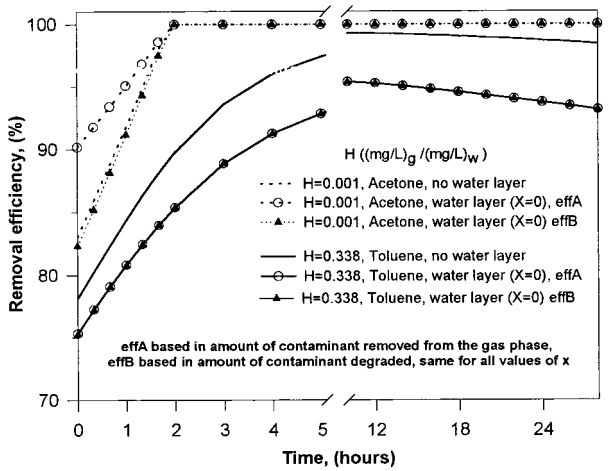


**FIGURE 6. Effect of the amount of water recycled and the solubility of the contaminant.**

water layer is neglected. Since the amount of acetone dissolved in the water and discharged with it is high, the efficiency based on the amount of contaminant removed from the gas phase is higher than the one based on the amount of contaminant biologically removed. When the water layer is neglected, the reactor efficiency is very close to the one including the water layer based on the amount of contaminant degraded. The liquid layer presents low mass transfer resistance for a high solubility compound. The conclusion of this study is that the reactor removal efficiency has to be carefully defined when dealing with highly soluble compounds and partial recycle of the liquid nutrient flow, because the amount of compound discharged with the water can be significant compared to the amount biologically degraded.

## Acknowledgments

This research has been sponsored in part by a grant from the U.S. Army Construction Engineering Research Laboratory.

## Nomenclature

| | |
|---|---|
| $a_0$, $a_f$ | specific surface area per unit volume of reactor, for clean bed and for bed with biofilm ($cm^{-1}$) |
| $b$, $b_d$, $b_s$ | shear/decay, decay, and shear rate coefficients, respectively ($s^{-1}$) |
| $C_f$, $C_w$, $C_g$ | biofilm, water phase, and gas-phase VOC concentrations (g COD/$cm^3$) |
| $C_{g0}$ | inlet gas-phase VOC concentration (g COD/$cm^3$) |
| $D_f$, $D_w$ | VOC diffusivity in the biofilm and in water, respectively ($cm^2/s$) |
| $H$ | Henry's law constant $((mg/L)_g/(mg/L)_w)$ |
| $K_s$ | Monod saturation constant (g COD/L) |
| $L$ | equivalent pipe radius or distance from the wall of the channel to the center (cm) |
| $L_f$, $L_w$ | biofilm and water layer thickness (cm) |
| $M_{gi}$, $M_{ge}$ | mass of contaminant in influent and effluent gas phase (g) |
| $M_{we}$ | mass of contaminant that leaves the biofilter in the effluent water that is not recycled (g) |
| $n$ | number of characteristic packing spheres in contact with a given one |
| $Q_g$, $Q_w$ | gas and water flow rate ($cm^3/s$) |
| $r_d$ | ratio between VOC diffusivities in biofilm and water |
| $R_p$ | characteristic packing sphere radius (cm) |
| $u_0$ | approach velocity to the biofilter (cm/s) |
| $v_g$, $v_w$ | velocities of gas and water phase (cm/s) |
| $\bar{v}_g$, $\bar{v}_w$ | average velocities of gas and water phase (cm/s) |
| $v_i$ | water-gas interface velocity |
| $X$ | faction of the nutrient flow recycled in the system |
| $X_f$ | biomass density (g COD/$cm^3$) |
| $Y$ | yield coefficient (g COD biomass/g COD VOC) |

**Greek Letters**

| | |
|---|---|
| $\epsilon_0$, $\epsilon_f$ | clean bed porosity and bed porosity with biofilm |
| $\phi$ | sphericity of packing solids |
| $\mu_m$ | maximum growth rate ($s^{-1}$) |

## Literature Cited

(1) Jennings, P. A.; Snoeyink, V. L.; Chian, E. S. K. *Biotechnol. Bioeng.* **1976**, *18*, 1249−1273.
(2) Ottengraf, S. P. P.; Van der Oever, A. H. C. *Biotechnol. Bioeng.* **1983,** *25*, 3089−3102.
(3) Shareefdeen, Z.; Baltzis, B. C.; Oh, Y. S.; Bartha, R. *Biotechnol. Bioeng.* **1993,** *41*, 512−524.
(4) Shareefdeen, Z.; Baltzis, B. C. *Chem. Eng. Sci.* **1994,** *49* (24A), 4347−4360.
(5) Zarook, S. M.; Shaikh, A. A.; Ansar, Z. *Chem. Eng. Sci.* **1997,** *52* (5), 759−773.
(6) Deshusses, M. A.; Hamer, G.; Dunn, I. J. *Environ. Sci. Technol.* **1995**, *29*, 1048−1058.
(7) Deshusses, M. A.; Hamer, G.; Dunn, I. J. *Environ. Sci. Technol.* **1995**, *29*, 1059−1068.
(8) Alonso, C.; Suidan, M. T.; Sorial, G. A.; Smith, F. L.; Biswas, P.; Smith, P. J.; Brenner, R. C. *Biotech. Bioeng.* **1997**, *54*, 583−549.
(9) Sorial, G. A.; Smith, F. L.; Suidan, M. T.; Biswas, P.; Brenner, R. C. *J. Air Waste Manage. Assoc.* **1995**, *45*, 801−810.
(10) Smith, F. L.; Sorial, G. A.; Suidan, M. T.; Breen, A. W.; Biswas, P.; Brenner, R. C. *Environ. Sci. Technol.* **1996**, *30*, 1744−1751.
(11) Rittmann, B. E. *Biotechnol. Bioeng.* **1982**, *42*, 501−506.
(12) Peyton, B. M.; Characklis, W. G. *Biotechnol. Bioeng.* **1993**, *41*, 728−735.
(13) Dullien, F. A. L. *Porous Media. Fluid Transport and Pore Structure;* Academic Press: New York, 1979.

*Received for review December 18, 1997. Revised manuscript received July 14, 1998. Accepted July 15, 1998.*

ES9711021